Article

Virtual Screening for Transition State Analogue Inhibitors of IRAP Based on Quantum Mechanically Derived Reaction Coordinates

Fredrik Svensson,[†] Karin Engen,[†] Thomas Lundbäck,[‡] Mats Larhed,[§] and Christian Sköld*,[†]

[†]Organic Pharmaceutical Chemistry, Department of Medicinal Chemistry, BMC, Uppsala University, P.O. Box 574, SE-751 23 Uppsala, Sweden

[‡]Chemical Biology Consortium Sweden, Science for Life Laboratory, Division of Translational Medicine and Chemical Biology, Department of Medical Biochemistry and Biophysics, Karolinska Institutet, Tomtebodavägen 23A, SE-171 65 Solna, Sweden

[§]Science for Life Laboratory, Department of Medicinal Chemistry, BMC, Uppsala University, P.O. Box 574, SE-751 23 Uppsala, Sweden

Ⓢ *Supporting Information*

ABSTRACT: Transition state and high energy intermediate mimetics have the potential to be very potent enzyme inhibitors. In this study, a model of peptide hydrolysis in the active site of insulin-regulated aminopeptidase (IRAP) was developed using density functional theory calculations and the cluster approach. The 3D structure models of the reaction coordinates were used for virtual screening to obtain new chemical starting points for IRAP inhibitors. This mechanism-based virtual screening process managed to identify several

known peptidase inhibitors from a library of over 5 million compounds, and biological testing identified one compound not previously reported as an IRAP inhibitor. This novel methodology for virtual screening is a promising approach to identify new inhibitors mimicking key transition states or intermediates of an enzymatic reaction.
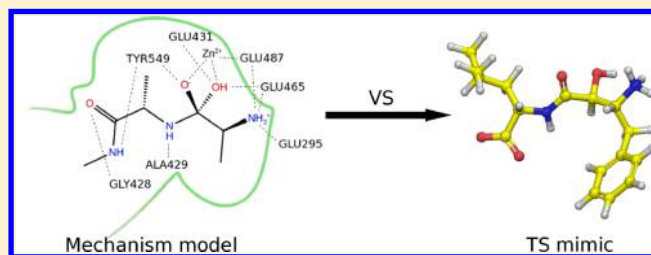
■ INTRODUCTION

Enzymes are important drug targets and approximately one-third of the marketed drugs target enzymes.[1] Enzymes are essential for many biochemical processes since they provide a reaction pathway with lower activation energy compared to the uncatalyzed reaction, typically by stabilizing the transition state (TS). By designing inhibitors that closely resemble the TS or a high energy intermediate, very strong binding can be achieved. Traditionally, this is considered to be due to tighter binding of the TS structure compared to the substrate, but more recent theories also suggest a dynamic factor where the TS analogs capture the dynamic features of the protein TS into a thermodynamically stable complex.[2−7] TS analogue inhibitors are known for a variety of targets and are also on the market as drugs against several indications, maybe most notably HIV protease and influenza neuraminidase.[8]

Virtual screening (VS) is today readily applied in drug discovery and a wealth of different methods have been reported.[9,10] However, the computational screening for TS- or intermediate analogues is still not well developed. This is largely because the structure of the TS or high energy intermediates cannot be experimentally determined using for example X-ray crystallography. Although the experimentally determined structures may be out of reach, TS structures can be accessed through computational methods, and TSs derived from such approaches have been used to obtain new inhibitors. Schramm and co-workers have reported several impressive examples where calculated TSs are used for the design of new

inhibitors with great success.[11,12] Also, the combination of a computationally derived TS structure and VS has previously been employed by Whalen et al. in order to facilitate structure based screening against glutamate racemase.[13]

One limiting factor to computationally derived TS models is the size of the systems. The large number of atoms that constitutes the active site and the substrate makes enzymatic reactions difficult to investigate using high level methods. To circumvent this, two different methods are commonly used. One approach is the use of QM/MM where a large part of the system is described using molecular mechanics and the catalytic site using quantum mechanics.[14] The second strategy, known as the cluster approach, uses only a limited number of atoms to represent the active site and treats the entire system with quantum mechanical methods.[15,16] Several successful applications of the cluster approach to metalloenzymes are present in the literature.[17] Even though this approach has been shown to be a valuable tool for modeling enzyme reactions, some limitations are inherent to the method. Since only a very limited part of the enzyme is considered, long-range interactions are not accounted for.[18] Care also has to be taken when optimizing the system to avoid artificial distortions and that a sufficient portion of the protein is considered.[19,20]

Insulin-regulated aminopeptidase (IRAP) is a membrane-anchored enzyme which has emerged as a promising target to

enhance cognitive functions. Drugs targeting IRAP can thus have an impact for treating dementia and other cognitive disorders.[21−23] It has previously been reported that VS based on a homology model of IRAP successfully can be used to identify new inhibitors.[24]

Aminopeptidase N (APN), endoplasmic reticulum aminopeptidase (ERAP), and IRAP are closely related enzymes belonging to the M1 family of peptidases.[25] The catalytic mechanism in the M1 family is fairly well understood due to a number of solved crystal structures.[26−29] There are a several TS mimetics that inhibit the M1 family of aminopeptidases, and of these, amastatin and bestatin (1 and 2, respectively, Scheme 1) have previously been tested and verified to be active against IRAP.[30]

Scheme 1. Structure of the Known Aminopeptidase TS Mimetics Amastatin 1 and Bestatin 2
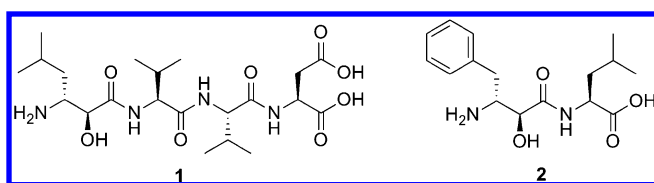
Previous experimental studies have proposed a reaction mechanism for APN as well as for ERAP. The mechanism (Figure 1) is believed to be essentially preserved across the enzymes and centers on activation of the bound substrate by an interaction between Zn^{2+}, a Tyr residue, and the carbonyl oxygen of the scissile peptide bond.[26,28,29] This enables the attack from a water molecule held in the vicinity of the activated peptide bond by two glutamic acids.

Based on the reaction mechanism above, we set out to model the reaction in the active site of IRAP using density functional theory (DFT) calculations and the cluster approach. From the calculated reaction model, key intermediate structures were used for docking and building of pharmacophore models in order to query a large collection of commercially available compounds for potential IRAP inhibitors with a specific focus on TS and intermediate mimics.

RESULTS AND DISCUSSION

Since no 3D structure was available for IRAP at the time of the investigation, the active site model was created based on the crystal structure of human APN (PDB ID 4FYR[28]). This structure was chosen due to its high sequence identity to IRAP in the catalytic site and its high resolution (1.91 Å). Sequence alignment identified two amino acids that differed between the investigated parts of the proteins. In IRAP, Gln213 and Val385 are represented by Glu295 and Ile461, respectively, and these amino acids were accordingly transformed to reflect the IRAP sequence. The water molecule necessary for the reaction was not present in the crystal structure but was added to the complex based on the previously described mechanism and was placed to interact with Glu431 and Glu465.[28,29] As a prototypical substrate, a di-Ala peptide with an N-Me amide capping group (3) was chosen. The final model contained 227 atoms representing the active site, including 11 amino acid side chains, backbone atoms, and the model substrate.

Scheme 2. Structure of the N-Me Amide Capped di-Ala Model Substrate 3
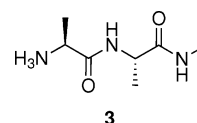

During the course of our work, two crystal structures of IRAP were released (PDB ID 4PJ6 and 4P8Q, resolution 2.96 and 3.02 Å, respectively).[31] A comparison between the 3D structures showed as expected a very high degree of similarity for most parts of the system included in this investigation. In the IRAP 3D structure, Zn^{2+} and the anchoring amino acids overlay very closely to related M1 aminopeptidases, and the catalytically essential Glu465 is in an identical position as the equivalent residues of ERAP1 and ERAP2.[31] Despite the similarities of the catalytic site to the previous M1 family structures, there are still some notable differences. The crystal structures of IRAP adopt an intermediate conformation between the open and closed form known from crystals of ERAP1.[26] No substrate or inhibitor is present in the structures; instead the substrate pockets are holding a single free amino acid residue. In the crystallized conformation, Tyr549, known to stabilize the substrate, does not form an interaction with the cocrystallized amino acid in the active site. Also, in this conformation the Gly-Ala-Met-Glu-Asn loop that forms part of the active site is shifted and adopts a somewhat different conformation. How big this difference is in the closed conformation with a bound substrate is however difficult to assess. Due to the active site similarities between APN and IRAP and neither of the currently available crystal structures of IRAP being in a closed conformation, we believe that an APN based model of IRAP provides a good starting point for the modeling of the catalyzed peptide hydrolysis.

Based on the proposed mechanism (Figure 1) and the active site model built from the APN 3D structure, the catalytic reaction was investigated by means of DFT calculations. The optimized geometry for the starting complex I is shown in Figure 2. In this configuration, the substrate N-terminal is
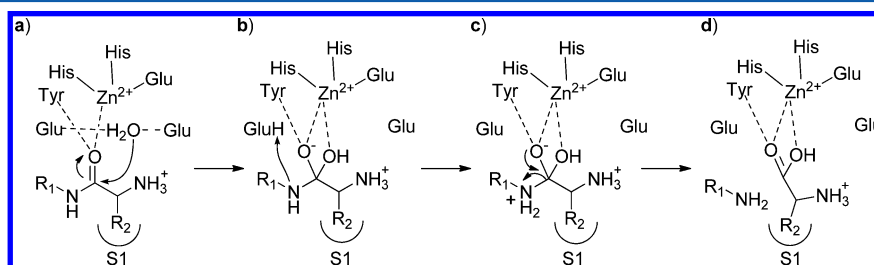

Figure 1. Proposed mechanism of APN and ERAP.
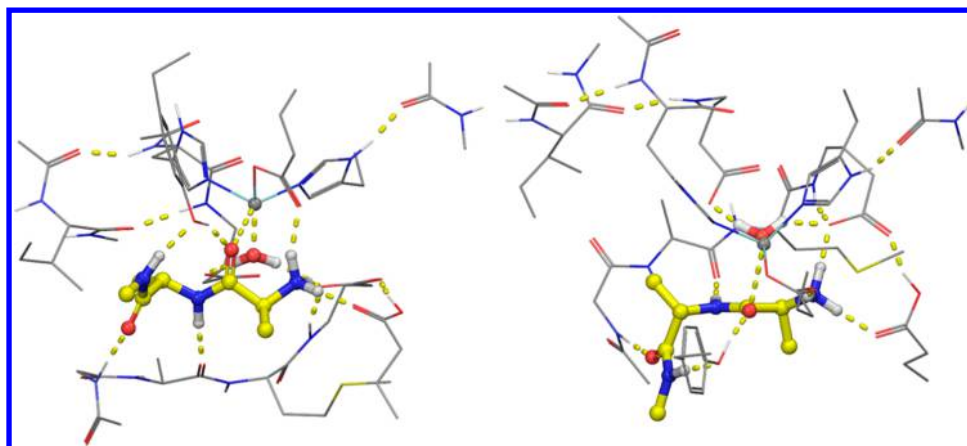
Figure 2. Optimized geometry for complex **I**. The model substrate **3** shown with yellow carbons. Shown in side and top views.
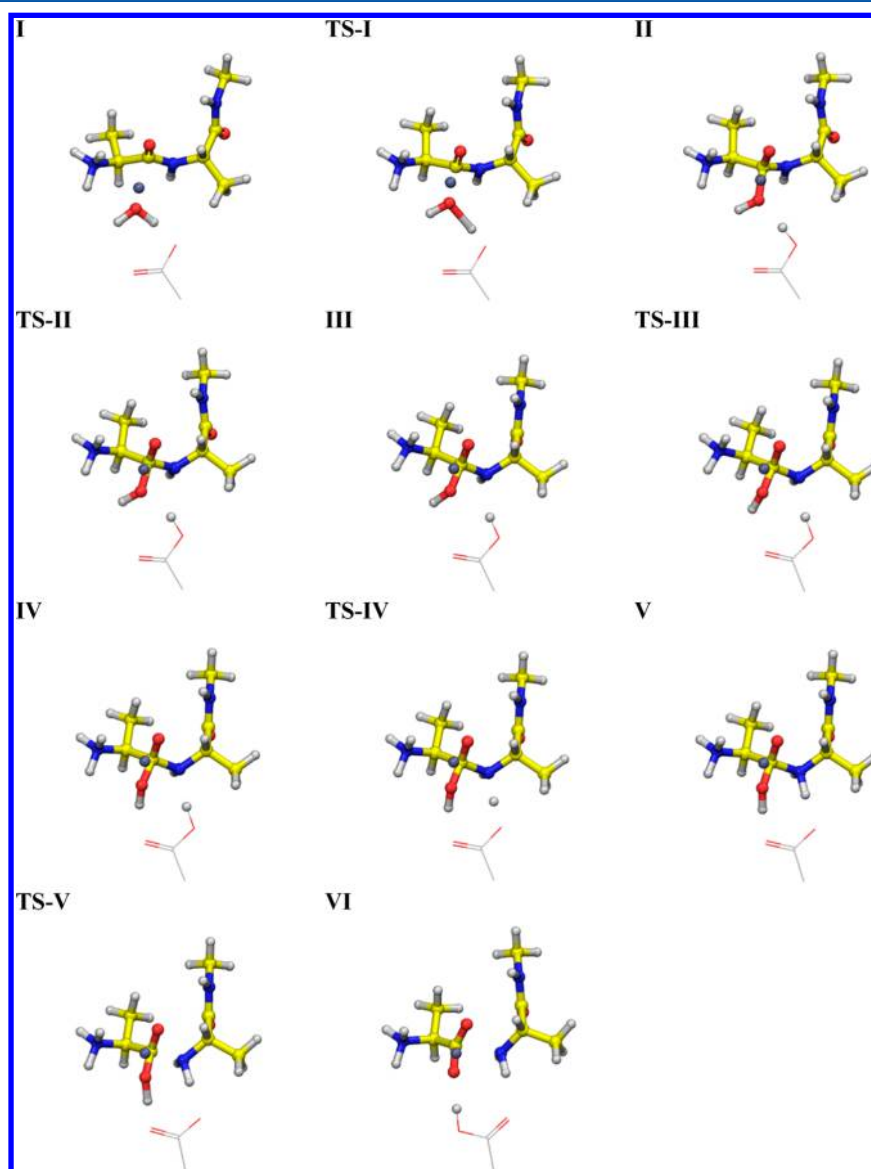
Figure 3. Calculated reaction steps for peptide hydrolysis catalyzed by IRAP. For clarity, only substrate **3**, the reacting water, Zn^{2+}, and part of Glu465 are shown. Steps **I** to **III** correspond to step a in Figure 1. Steps **III** to **V** correspond to b. **V** and **TS-V** correspond to step c, and the formed product **VI** corresponds to step d.
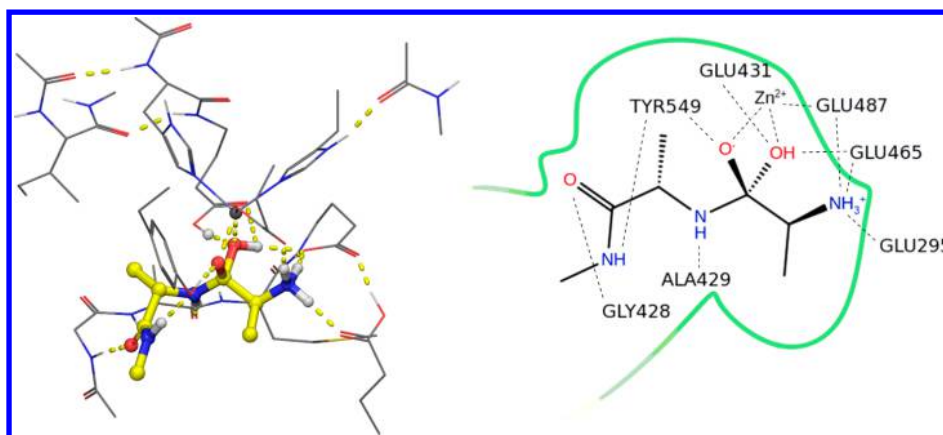
Figure 4. Interactions of intermediate **II**. Left hand side shows the full optimized geometry of **II** with all model atoms shown (nonpolar hydrogen atoms are omitted for clarity). Right hand side shows a schematic representation of **II** with the amino acids that make hydrogen bonds to the substrate annotated.
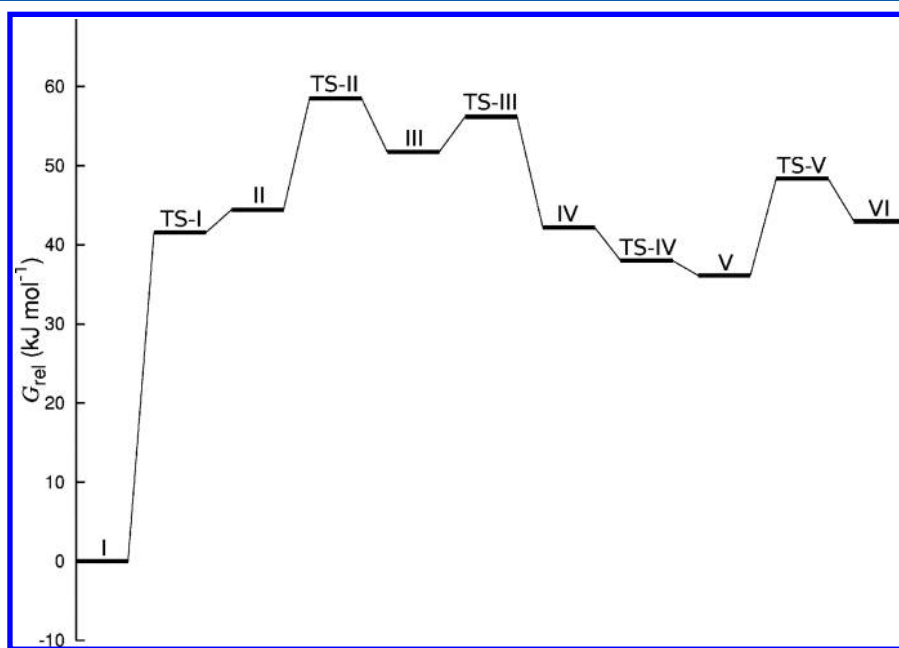
Figure 5. Calculated free energy pathway for peptide hydrolysis catalyzed by IRAP.

locked into place by interactions with Glu295, Glu465, and Glu487 with the amide carbonyl interacting with Zn^{2+}.

Reaction coordinates with parts of the structures shown are depicted in Figure 3 (figures of all steps with the full model are available in the Supporting Information). From the starting complex **I**, a concerted nucleophilic attack on the carbonyl group by the water and deprotonation by Glu465 forms the high-energy geminal diol intermediate **II**. The substrate protein interactions of **II** are shown in Figure 4. As part of the proton transfer from water to the amide nitrogen, the hydrogen bond between Glu465 and the formed hydroxyl is switched via **TS-II**. This step constitutes the highest calculated energy in the reaction pathway. Before protonation of the amine, the direction of the newly formed hydroxyl changes to form a hydrogen bond with Glu389. From this step (**IV**), the protonation of nitrogen takes place (**TS-IV**) forming the intermediate **V**, ready for cleavage of the scissile bond. Bond breakage and simultaneous deprotonation of the gem-diol results in the cleaved products in complex **VI**. The processes for product release and subsequent binding of a new substrate were

not included in the calculations. Overall, this mechanism model is in close agreement with the previously proposed mechanism.

The free energy profile of the reaction is shown in Figure 5. The free energy requirement from **I** to **TS-II** was calculated to 58.5 kJ mol^{-1}, making it the rate limiting step in our model.

The next step was to utilize the reaction mechanism for VS in order to screen for compounds mimicking key points in the reaction pathway. The VS was conducted in two steps. All compounds were docked against the active site model and subsequently subjected to a rigid pharmacophore screen using relevant features from the TS and high energy intermediates.

To conduct the docking study, we replaced the crystal structure active site with the DFT geometry optimized models. The structures of reaction complexes **II** and **V** were selected for docking, thus capturing the features of the two main reaction steps associated with the large change in substrate structure, namely the initial nucleophilic attack of water and the cleaving of the peptide, respectively. These two structures also have markedly different hydrogen bond directions that could result in the identification of different ligand classes during docking.

The intermediates **II** and **V** are also close both in energy and in structure to the TSs and should also benefit from strong stabilization from the enzyme.

Since we were primarily interested in compounds that could mimic structures in the reaction path, pharmacophore filtering of the docked poses was performed. Aside from enriching compounds that have similar interactions as the reaction intermediates, pharmacophore filtering may enhance the chance of finding active compounds.[32] A key feature of the mechanism is the gem-diol structure formed after the initial reaction with the water. Since this feature is not present in the substrate, but is in all reaction intermediate steps, it presents a highly relevant structural motif that cannot be identified in the unreacted substrate. Another key feature present throughout the mechanism is the strong electrostatic interactions of the N-terminal, anchoring the substrate in the active site.[29] Based on these features, three pharmacophore features were chosen, two hydrogen bond acceptors for the zinc-interacting oxygen atoms and one positive charge at the position of the N-terminal. We chose to base the pharmacophore on the substrate structure in complex **II** (Figure 6). Because the chosen features are present
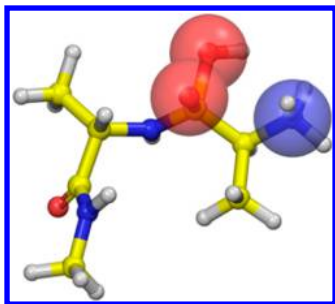
Figure 6. Visual representation of the high energy intermediate-based pharmacophore. Red spheres represent hydrogen bond acceptors; the blue sphere represents positive charge.

throughout the investigated part of the reaction and the relative large allowance in the pharmacophore search, the results are expected to be similar regardless of which complex the pharmacophore is based on.

The two dockings resulted in 25 074 704 scored structures, but only a small fraction of the docked compounds passed the pharmacophore filter. When the results from the two dockings were combined, a total of 3974 unique compounds remained

after the pharmacophore filtration. We aimed to limit the hit list to about 1000 molecules for the manual inspection of the docking poses. A total of 1102 structures had a docking score better or equal to −7, and we chose to limit the manual inspection to these. However, in order to identify any structures that might not pass the pharmacophore filter but still be predicted as an exceptionally good binder, the top 500 compounds from each docking run were also manually reviewed. We also calculated the ligand efficiency, as the docking score per non-hydrogen atom, to enhance the scoring of fragment-like compounds that may be useful chemical starting points for the development of new inhibitors.

Gratifyingly, the VS process resulted in the identification of several hits with structural features and binding poses that were plausible mimics of the TS and high energy intermediates. Among the top scoring compounds, we were able to locate both **1** (pharmacophore filtered rank 155) and **2** (pharmacophore filtered rank 45), which are known aminopeptidase TS mimetic inhibitors.[33] Also among the hits were examples of known phosphinate-based APN inhibitors[34] and apstatin,[35] an aminopeptidase P inhibitor. The identification of several known peptidase inhibitors of different compound classes that have structural features that can mimic the TS and intermediates shows that this VS approach has a high potential of identifying TS- and high energy intermediate mimicking inhibitors.

To assess the impact of including the information about the reaction intermediate binding mode in the VS process, we compared the results before and after the pharmacophore filter in more detail. Since only a few compounds with TS mimicking structural features and confirmed IRAP inhibition are known, the analysis was limited to compounds **1** and **2**. Although this is a very small test set, the analysis should provide some indication regarding the effect from the pharmacophore filter. When only the unfiltered docking results were considered, the binding poses found for compounds **1** and **2** after the pharmacophore filtration received ranks of 512 160 and 365 394, respectively. This is in stark contrast to the filtered ranks 155 and 45, respectively. Furthermore, the pharmacophore filter ensures that relevant binding modes are obtained from VS. The binding mode of **2** obtained from VS shows similar interaction possibilities as the gem-diol reaction intermediate and is highly similar to the experimental binding mode of **2** as found cocrystallized with APN (RMSD = 1.39 Å when superimposing all heavy atoms), as seen in Figure 7.
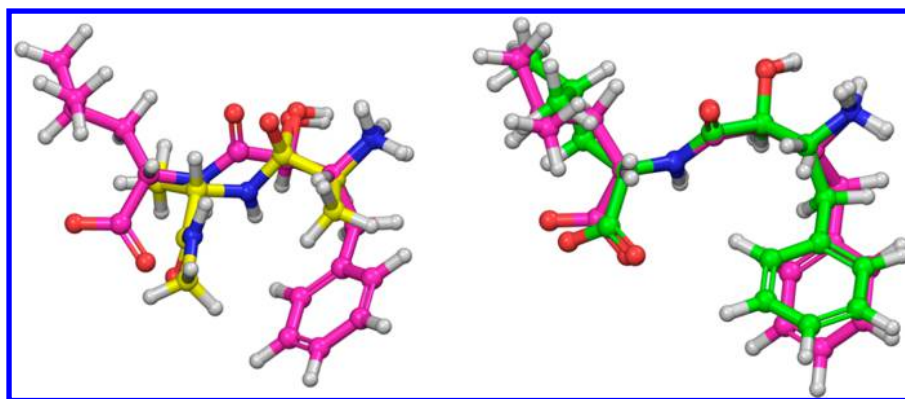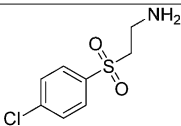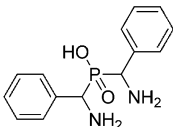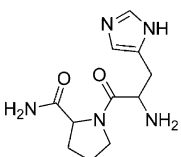
Figure 7. Left-hand side shows **2** (pink carbons) in the binding pose identified from the VS overlaid to the substrate **3** (yellow carbons) from intermediate **II**. Right-hand side shows **2** (pink carbons) in the binding pose identified from the VS superimposed on **2** (green carbons) cocrystallized with APN (PDB ID 4FKK).

Thus, the results show that the pharmacophore filter, keeping only the compounds with the key interaction identified from the reaction model, is crucial in order to identify the known TS mimetic inhibitors in a binding pose that resembles a stage in the reaction mechanism.

Seven potential novel binders were selected, acquired, and biochemically evaluated (Table 1). The seven structures were
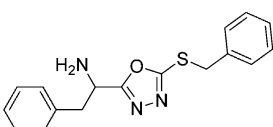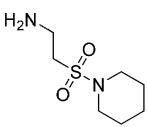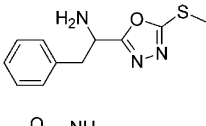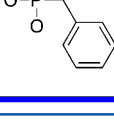
Table 1. Structures of the Compounds Chosen for Biochemical Evaluation

Number	Structure	Assay result
4		Inactive
5		Inactive
6		Inactive
7		Inactive
8		Inactive
9		Inactive
10		IC$_{50}$ = 230 (± 7) μM

selected for their similarity to the reaction intermediates, but care was also taken to include different chemotypes. In addition, we also included **1** in the biochemical evaluation as a positive control. The testing identified amino(phenyl)-methylphosphonic acid, (**10**, Table 1, ligand efficiency docking rank 36 against complex **V**) as an inhibitor of IRAP with an IC$_{50}$ of 230 (±7) μM. The biochemical assay also confirmed **1** as an IRAP inhibitor, and the IC$_{50}$ was recorded at 26 (±0.6) μM.

The identification of **10** as an IRAP inhibitor was rewarding as the small fragment-like inhibitor represents a highly suitable chemical starting point for future chemical development into potent IRAP inhibitors. Although not shown previously to be inhibitors of IRAP, α-aminophosphonic acids have previously

been developed into high affinity APN inhibitors.[36] While not very potent, the identified inhibitor closely resembles the substrate structure in **II** (Figure 8). The low potency of the hit might partly be explained by the small size of the inhibitor compared to the IRAP substrates, making it difficult to achieve sufficient interactions.
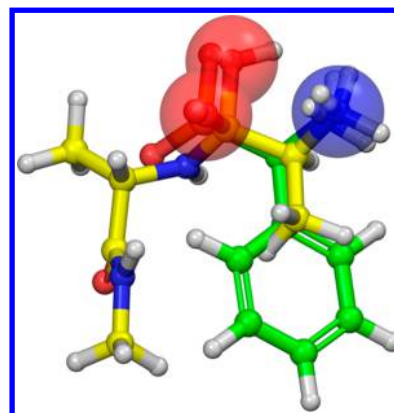
Figure 8. Docked pose of **10** overlaid on the pharmacophore and **3** from intermediate **II**.

The use of VS to identify TS or high-energy intermediate mimetics is possibly made more difficult by the fact that the compound databases used might not include structures able to perfectly mimic the reaction coordinate of interest. In some cases, it might not even be possible to synthesize a molecule that perfectly matches the properties of the TS.[12] Even though this approach might not result in the very tight binding inhibitors that could be achieved by perfect mimicry of the TS, the located inhibitors might still be promising starting points for further development and represent structure classes that would not have been considered in traditional approaches.

Overall, the presented protocol for VS aiming to identify enzymatic reaction coordinate mimetics is promising. The findings reported in this paper are the first step toward validating this method. We hope that in future applications the protocol will yield inhibitors also for new enzyme classes where TS-/intermediate-based inhibitors are not previously known. Efforts are ongoing in our laboratory to extend the application of this VS protocol to additional targets.

■ CONCLUSIONS

In this investigation, we present a detailed view of the mechanism of IRAP, derived by means of DFT calculations and the cluster approach. The mechanism follows the overall pathway previously described for the M1 family of peptidases and with reasonable energy requirements for the calculated steps.

The VS protocol presented herein provides a promising method for identifying compounds mimicking TSs and high energy intermediates in enzymatic reactions. Although the protocol includes rigorous modeling of the enzymatic reaction, the information gained is highly valuable. First, the protein used in the docking investigation will correspond to a highly relevant structure that stabilizes the TS and high energy intermediates and is devoid of any induced fit provided by a cocrystallized ligand. Second, information on the spatial orientation of functional groups highly suitable for protein interaction is provided by the model of the TSs and high energy

intermediates in the reaction coordinates. This information provides an important filter for extracting high quality potential ligands from the docking results.

A number of peptidase inhibitors were identified using this VS method, and biological testing identified one compound, amino(phenyl)methylphosphonic acid (**10**), not previously reported as an IRAP inhibitor. Overall, the presented method provides significant new information on the biological target and is a useful alternative to traditional screening methods for identifying new classes of enzyme inhibitors.

■ MATERIALS AND METHODS

Computational Methods. Sequence alignment between APN (UniProt identifier P15144) and IRAP (UniProt identifier Q9UIQ6) was performed using ClustalW2 (accessed April 22, 2014).[37,38]

The crystal structure of human APN (PDB ID 4FYR[16]) was downloaded from the protein data bank[20] (PDB). The protein was prepared using Schrödinger Suite 2012 Protein Preparation Wizard.[21−23] This included preprocessing of the protein structure, generation of ionization and tautomeric states, automatic optimization of the hydrogen bond network, and a restrained minimization of hydrogen atom positions. All settings were kept at default except for the restrained minimization that was restricted to hydrogens only.

All DFT calculations, both geometry optimizations and single point calculations, were performed with Jaguar[39,40] using the B3LYP[41−43] hybrid functional and the LACVP* basis set[44] (applying 6-31G*[45−50] for the system investigated in this study). Geometry optimization was carried out with all protein backbone C_α atoms frozen (see Supporting Information for frozen coordinates) using the built in loose convergence criteria in Jaguar. Based on the gas phase optimized structures, single point solvation energies were calculated using the PBF[51,52] solvation model using parameters for water but using a dielectric constant of 4, a common approach in protein modeling. For systems as large as the one investigated herein, previous studies have shown that the value of the dielectric constant has only a very small influence on the energies.[53−55] Dispersion corrections were calculated using the DFT-D3 program from the optimized structures.[56] The final energies were derived by summing the solution phase energy, the dispersion correction, and the thermodynamic vibrational contribution at 298.15 K. All TSs were verified to be connected to the respective proceeding and preceding mimimas using QRC.[57] The frozen coordinates in the model give rise to a small number of imaginary frequencies of a low magnitude. These frequencies do, however, remain relatively constant throughout the reaction and are expected to have only a small influence on the calculated energies.

The geometries for **II** and **V** were also calculated using the B3LYP-D3 functional in Jaguar in order to verify that the geometry difference is sufficiently small not to have a major impact on the VS process. Overall the optimization produced similar geometries for both **II** and **V** to those obtained using B3LYP (RMSD = 0.2107 and 0.2495, respectively). The optimized coordinates are available in the Supporting Information.

For VS, the eMolecules Plus database (www.emolecules. com) was used. The database included at time of download (July 14, 2014) about 5.6 million chemical structures. Prior to VS, all compounds were submitted to LigPrep,[58,59] generating tautomers, stereoisomers, and protonation states. This resulted

in 14 644 844 structures. All the structures with a molecular weight higher than 600 were removed from the data set, leaving 14 238 430 structures that were used in the docking calculations.

The protein was prepared for docking by replacing the active site of the crystal structure with the active site model derived from the DFT calculations. Subsequently, the protein was submitted to receptor grid generation in Glide, using the default settings generating a grid centered on the substrate (see the Supporting Information for a full list of Glide grid generation input file options). Docking was conducted using Glide[60−62] SP, using the default settings and saving only the best pose for each input structure (see Supporting Information for a full list of Glide input file options).

Phase[63,64] was used for pharmacophore generation and screening. The default matching criteria of 2 Å was used during the screening with the requirement that hits need to match all three features. All the compounds were screened using the pharmacophore in their docked conformation using the "score in place" option in phase.

Graphics for this paper were prepared using PyMol 1.6.[65]

Enzymatic Assay. The enzymatic assay was based on membrane preparations from Chinese hamster ovary (CHO) cells as a source of IRAP activity, and it was used to measure the inhibition abilities of the compounds at a range of different concentrations (see Borhade et al.[23] for details). The CHO cells are known to abundantly express IRAP and contain minimal amounts of contaminating APN activities.[66] The extent of enzymatic activity in each sample was quantified in a 96-well microtiter plate (Nunc, product no. 269620) using the peptide-like substrate L-leucine-*p*-nitroanilide (L-Leu-*p*NA; Sigma-Aldrich, product no. L9125), which upon IRAP mediated hydrolysis produces *p*-nitroaniline that absorbs at 405 nm. The final assay volume was 200 µL in an assay buffer consisting of 50 mM Tris-HCl, 150 mM NaCl, and 0.1 mM phenyl-methanesulfonylfluoride (PMSF) at pH 7.4. The assay was conducted in the presence of a final concentration of 1 mM L-Leu-*p*NA and CHO cell membranes from approximately 220 000 cells per well. The CHO membrane preparation was performed as described by Demaegt et al., with the lysis of washed cells being conducted by means of ultrasonication followed by multiple strokes (>20) with a Dounze homogenizer and a centrifugation (30 000*g* for 30 min at 4 °C) procedure for pelleting and washing the membranes.[67] The protocol for running the dose−response assay started with dissolving the compounds in the assay buffer (10−58 mM depending on solubilities), followed by serial dilution in buffer by a factor of 1/2 in columns 1 through 11 in a U-formed 96-well plate (Nunc, product no. 267245). Column 12 was reserved for controls with the equivalent amount of buffer added to wells A12−D12 (negative control, 0% inhibition of the enzyme) and a 500 µM solution of *N*-(3-(1*H*-tetrazol-5-yl)phenyl)-4-bromo-5-chlorothiophene-2-sulfonamide[23] (0.5% DMSO) added to wells E12−H12 (positive control, 100% inhibition of the enzyme). The diluted compound solutions and controls were then transferred to assay plates in triplicate (50 µL to each well), followed by the addition of diluted homogenized CHO cell membranes (50 µL) and substrate (100 µL) to initiate the enzymatic reaction. The plates were covered with lids and then incubated at room temperature for 17 h. Raw data from the absorbance measurements were then imported into Microsoft Excel for a conversion to % inhibition data based on the controls on each plate. The curves were

thereafter fitted to a four-parameter dose−response model within XLfit (model 205) to obtain best-fit values for the IC$_{50}$ value, Hill slope, and the upper and lower limits of the dose−response curve.

Commercially available compounds for testing were acquired from Sigma-Aldrich. These included amastatin (LOT 088 K8740 V, ≥ 97% purity (HPLC) according to CoA) and amino(phenyl)metylphosphonic acid (NMR spectra available in the SI).

ASSOCIATED CONTENT

Ⓢ Supporting Information

The Supporting Information is available free of charge on the ACS Publications website at DOI: 10.1021/acs.jcim.5b00359.

> XYZ coordinates, Jaguar zmat sections, and energies for the reaction complexes. Glide grid generation options and Glide input file options. Sequence alignment between APN and IRAP. NMR determination of compound **10**. Curves for the IC50 measurements (PDF)

AUTHOR INFORMATION

Corresponding Author

*Phone: +46-18-4714394. E-mail: christian.skold@orgfarm.uu.se.

Author Contributions

The manuscript was written through contributions of all authors. All authors have given approval to the final version of the manuscript.

Notes

The authors declare no competing financial interest.

ABBREVIATIONS USED

APN, aminopeptidase N; CHO, Chinese hamster ovary; ERAP, endoplasmic reticulum aminopeptidase; IRAP, insulin regulated amino peptidase; MM, molecular mechanics; QM, quantum mechanics; VS, virtual screening

REFERENCES

(1) Imming, P.; Sinning, C.; Meyer, A. Drugs, Their Targets and the Nature and Number of Drug Targets. *Nat. Rev. Drug Discovery* **2006**, *5*, 821−834.

(2) Lienhard, G. E. Enzymatic Catalysis and Transition-State Theory. *Science* **1973**, *180*, 149−154.

(3) Schramm, V. L. Enzymatic Transition States and Transition State Analogues. *Curr. Opin. Struct. Biol.* **2005**, *15*, 604−613.

(4) Wolfenden, R. Transition State Analogues for Enzyme Catalysis. *Nature* **1969**, *223*, 704−705.

(5) Wolfenden, R. Analog Approaches to the Structure of the Transition State in Enzyme Reactions. *Acc. Chem. Res.* **1972**, *5*, 10−18.

(6) Machleder, S. Q.; Pineda, J. R. E. T.; Schwartz, S. D. On the Origin of the Chemical Barrier and Tunneling in Enzymes. *J. Phys. Org. Chem.* **2010**, *23*, 690−695.

(7) Schwartz, S. D.; Schramm, V. L. Enzymatic Transition States and Dynamic Motion in Barrier Crossing. *Nat. Chem. Biol.* **2009**, *5*, 551−558.

(8) Gluza, K.; Kafarski, P. Transition State Analogues of Enzymatic Reactions as Potential Drugs. In *Drug Discovery*; El-Shemy, H., Ed.; InTech: Rijeka, Croatia, 2013.

(9) Tanrikulu, Y.; Krüger, B.; Proschak, E. The Holistic Integration of Virtual Screening in Drug Discovery. *Drug Discovery Today* **2013**, *18*, 358−364.

(10) Kar, S.; Roy, K. How Far Can Virtual Screening Take Us in Drug Discovery? *Expert Opin. Drug Discovery* **2013**, *8*, 245−261.

(11) Schramm, V. L. Enzymatic Transition States, Transition-State Analogs, Dynamics, Thermodynamics, and Lifetimes. *Annu. Rev. Biochem.* **2011**, *80*, 703−732.

(12) Schramm, V. L. Transition States, Analogues, and Drug Development. *ACS Chem. Biol.* **2012**, *8*, 71−81.

(13) Whalen, K. L.; Pankow, K. L.; Blanke, S. R.; Spies, M. A. Exploiting Enzyme Plasticity in Virtual Screening: High Efficiency Inhibitors of Glutamate Racemase. *ACS Med. Chem. Lett.* **2009**, *1*, 9−13.

(14) Senn, H. M.; Thiel, W. QM/MM Studies of Enzymes. *Curr. Opin. Chem. Biol.* **2007**, *11*, 182−187.

(15) Siegbahn, P. M.; Himo, F. Recent Developments of the Quantum Chemical Cluster Approach for Modeling Enzyme Reactions. *JBIC, J. Biol. Inorg. Chem.* **2009**, *14*, 643−651.

(16) Siegbahn, P. E. M.; Himo, F. The Quantum Chemical Cluster Approach for Modeling Enzyme Reactions. *Wiley Interdiscip. Rev. Comput. Mol. Sci.* **2011**, *1*, 323−336.

(17) Blomberg, M. R. A.; Borowski, T.; Himo, F.; Liao, R.-Z.; Siegbahn, P. E. M. Quantum Chemical Studies of Mechanisms for Metalloenzymes. *Chem. Rev.* **2014**, *114*, 3601−3658.

(18) Hu, L.; Eliasson, J.; Heimdal, J.; Ryde, U. Do Quantum Mechanical Energies Calculated for Small Models of Protein-Active Sites Converge?†. *J. Phys. Chem. A* **2009**, *113*, 11793−11800.

(19) Sumner, S.; Söderhjelm, P.; Ryde, U. Effect of Geometry Optimizations on QM-Cluster and QM/MM Studies of Reaction Energies in Proteins. *J. Chem. Theory Comput.* **2013**, *9*, 4205−4214.

(20) Hu, L.; Söderhjelm, P.; Ryde, U. On the Convergence of QM/MM Energies. *J. Chem. Theory Comput.* **2011**, *7*, 761−777.

(21) Andersson, H.; Hallberg, M. Discovery of Inhibitors of Insulin-Regulated Aminopeptidase as Cognitive Enhancers. *Int. J. Hypertens.* **2012**, *2012*, No. 7896711.

(22) Albiston, A. L.; Morton, C. J.; Ng, H. L.; Pham, V.; Yeatman, H. R.; Ye, S.; Fernando, R. N.; De Bundel, D.; Ascher, D. B.; Mendelsohn, F. A. O.; Parker, M. W.; Chai, S. Y. Identification and Characterization of a New Cognitive Enhancer Based on Inhibition of Insulin-Regulated Aminopeptidase. *FASEB J.* **2008**, *22*, 4209−4217.

(23) Borhade, S. R.; Rosenström, U.; Sävmarker, J.; Lundbäck, T.; Jenmalm-Jensen, A.; Sigmundsson, K.; Axelsson, H.; Svensson, F.; Konda, V.; Sköld, C.; Larhed, M.; Hallberg, M. Inhibition of Insulin-Regulated Aminopeptidase (IRAP) by Arylsulfonamides. *ChemistryOpen* **2014**, *3*, 256−263.

(24) Mountford, S. J.; Albiston, A. L.; Charman, W. N.; Ng, L.; Holien, J. K.; Parker, M. W.; Nicolazzo, J. A.; Thompson, P. E.; Chai, S. Y. Synthesis, Structure−Activity Relationships and Brain Uptake of a Novel Series of Benzopyran Inhibitors of Insulin-Regulated Aminopeptidase. *J. Med. Chem.* **2014**, *57*, 1368−1377.

(25) Agrawal, N.; Brown, M. A. Genetic Associations and Functional Characterization of M1 Aminopeptidases and Immune-Mediated Diseases. *Genes Immun.* **2014**, *15*, 521−527.

(26) Kochan, G.; Krojer, T.; Harvey, D.; Fischer, R.; Chen, L.; Vollmar, M.; von Delft, F.; Kavanagh, K. L.; Brown, M. A.; Bowness, P.; Wordsworth, P.; Kessler, B. M.; Oppermann, U. Crystal Structures of the Endoplasmic Reticulum Aminopeptidase-1 (ERAP1) Reveal the Molecular Basis for N-Terminal Peptide Trimming. *Proc. Natl. Acad. Sci. U. S. A.* **2011**, *108*, 7745−7750.

(27) Tholander, F.; Muroya, A.; Roques, B.-P.; Fournié-Zaluski, M.-C.; Thunnissen, M. M. G. M.; Haeggström, J. Z. Structure-Based Dissection of the Active Site Chemistry of Leukotriene A4 Hydrolase:

Implications for M1 Aminopeptidases and Inhibitor Design. *Chem. Biol.* **2008**, *15*, 920−929.

(28) Wong, A. H. M.; Zhou, D.; Rini, J. M. The X-Ray Crystal Structure of Human Aminopeptidase N Reveals a Novel Dimer and the Basis for Peptide Processing. *J. Biol. Chem.* **2012**, *287*, 36804−36813.

(29) Chen, L.; Lin, Y.-L.; Peng, G.; Li, F. Structural Basis for Multifunctional Roles of Mammalian Aminopeptidase N. *Proc. Natl. Acad. Sci. U. S. A.* **2012**, *109*, 17966−17971.

(30) Matsumoto, H.; Rogi, T.; Yamashiro, K.; Kodama, S.; Tsuruoka, N.; Hattori, A.; Takio, K.; Mizutani, S.; Tsujimoto, M. Characterization of a Recombinant Soluble Form of Human Placental Leucine Aminopeptidase/oxytocinase Expressed in Chinese Hamster Ovary Cells. *Eur. J. Biochem.* **2000**, *267*, 46−52.

(31) Hermans, S. J.; Ascher, D. B.; Hancock, N. C.; Holien, J. K.; Michell, B. J.; Chai, S. Y.; Morton, C. J.; Parker, M. W. Crystal Structure of Human Insulin-Regulated Aminopeptidase with Specificity for Cyclic Peptides. *Protein Sci.* **2015**, *24*, 190−199.

(32) Muthas, D.; Sabnis, Y. A.; Lundborg, M.; Karlén, A. Is It Possible to Increse Hit Rates in Structure-Based Virtual Screening by Pharmacophore Filtering? An Investigation of the Advantages and Pitfalls of Post-Filtering. *J. Mol. Graphics Modell.* **2008**, *26*, 1237−1251.

(33) Wilkes, S. H.; Prescott, J. M. The Slow, Tight Binding of Bestatin and Amastatin to Aminopeptidases. *J. Biol. Chem.* **1985**, *260*, 13154−13162.

(34) Drag, M.; Grzywa, R.; Oleksyszyn, J. Novel Hydroxamic Acid-Related Phosphinates: Inhibition of Neutral Aminopeptidase N (APN). *Bioorg. Med. Chem. Lett.* **2007**, *17*, 1516−1519.

(35) Prechel, M. M.; Orawski, A. T.; Maggiora, L. L.; Simmons, W. H. Effect of a New Aminopeptidase P Inhibitor, Apstatin, on Bradykinin Degradation in the Rat Lung. *J. Pharmacol. Exp. Ther.* **1995**, *275*, 1136−1142.

(36) Grzywa, R.; Sokol, A. M.; Sieńczyk, M.; Radziszewicz, M.; Kościołek, B.; Carty, M. P.; Oleksyszyn, J. New Aromatic Monoesters of A-Aminoaralkylphosphonic Acids as Inhibitors of Aminopeptidase N/CD13. *Bioorg. Med. Chem.* **2010**, *18*, 2930−2936.

(37) Larkin, M. A.; Blackshields, G.; Brown, N. P.; Chenna, R.; McGettigan, P. A.; McWilliam, H.; Valentin, F.; Wallace, I. M.; Wilm, A.; Lopez, R.; Thompson, J. D.; Gibson, T. J.; Higgins, D. G.; Clustal, W.; Clustal, X. Clustal W and Clustal X version 2.0. *Bioinformatics* **2007**, *23*, 2947−2948.

(38) Goujon, M.; McWilliam, H.; Li, W.; Valentin, F.; Squizzato, S.; Paern, J.; Lopez, R. A New Bioinformatics Analysis Tools Framework at EMBL−EBI. *Nucleic Acids Res.* **2010**, *38*, W695−W699.

(39) *Jaguar*, version 8.1; Schrödinger, LCC: New York, 2013.

(40) Bochevarov, A. D.; Harder, E.; Hughes, T. F.; Greenwood, J. R.; Braden, D. A.; Philipp, D. M.; Rinaldo, D.; Halls, M. D.; Zhang, J.; Friesner, R. A. Jaguar: A High-Performance Quantum Chemistry Software Program with Strengths in Life and Materials Sciences. *Int. J. Quantum Chem.* **2013**, *113*, 2110−2142.

(41) Becke, A. D. A New Mixing of Hartree−Fock and Local Density−functional Theories. *J. Chem. Phys.* **1993**, *98*, 1372−1377.

(42) Becke, A. D. Density-Functional Thermochemistry. III. The Role of Exact Exchange. *J. Chem. Phys.* **1993**, *98*, 5648−5652.

(43) Lee, C.; Yang, W.; Parr, R. G. Development of the Colle-Salvetti Correlation-Energy Formula into a Functional of the Electron Density. *Phys. Rev. B: Condens. Matter Mater. Phys.* **1988**, *37*, 785−789.

(44) Hay, P. J.; Wadt, W. R. Ab Initio Effective Core Potentials for Molecular Calculations. Potentials for K to Au Including the Outermost Core Orbitals. *J. Chem. Phys.* **1985**, *82*, 299.

(45) Ditchfield, R.; Hehre, W. J.; Pople, J. A. Self-Consistent Molecular-Orbital Methods. IX. An Extended Gaussian-Type Basis for Molecular-Orbital Studies of Organic Molecules. *J. Chem. Phys.* **1971**, *54*, 724.

(46) Hehre, W. J.; Pople, J. A. Self-Consistent Molecular Orbital Methods. XIII. An Extended Gaussian-Type Basis for Boron. *J. Chem. Phys.* **1972**, *56*, 4233.

(47) Binkley, J. S.; Pople, J. A. Self-Consistent Molecular Orbital Methods. XIX. Split-Valence Gaussian-Type Basis Sets for Beryllium. *J. Chem. Phys.* **1977**, *66*, 879.

(48) Hariharan, P. C.; Pople, J. A. The Influence of Polarization Functions on Molecular Orbital Hydrogenation Energies. *Theor. Chim. Acta* **1973**, *28*, 213−222.

(49) Hehre, W. J.; Ditchfield, R.; Pople, J. A. Self-Consistent Molecular Orbital Methods. XII. Further Extensions of Gaussian-Type Basis Sets for Use in Molecular Orbital Studies of Organic Molecules. *J. Chem. Phys.* **1972**, *56*, 2257.

(50) Francl, M. M.; Pietro, W. J.; Hehre, W. J.; Binkley, J. S.; Gordon, M. S.; DeFrees, D. J.; Pople, J. A. Self-Consistent Molecular Orbital Methods. XXIII. A Polarization-Type Basis Set for Second-Row Elements. *J. Chem. Phys.* **1982**, *77*, 3654.

(51) Marten, B.; Kim, K.; Cortis, C.; Friesner, R. A.; Murphy, R. B.; Ringnalda, M. N.; Sitkoff, D.; Honig, B. New Model for Calculation of Solvation Free Energies: Correction of Self-Consistent Reaction Field Continuum Dielectric Theory for Short-Range Hydrogen-Bonding Effects. *J. Phys. Chem.* **1996**, *100*, 11775−11788.

(52) Tannor, D. J.; Marten, B.; Murphy, R.; Friesner, R. A.; Sitkoff, D.; Nicholls, A.; Honig, B.; Ringnalda, M.; Goddard, W. A. Accurate First Principles Calculation of Molecular Charge Distributions and Solvation Energies from Ab Initio Quantum Mechanics and Continuum Dielectric Theory. *J. Am. Chem. Soc.* **1994**, *116*, 11875−11882.

(53) Sevastik, R.; Himo, F. Quantum Chemical Modeling of Enzymatic Reactions: The Case of 4-Oxalocrotonate Tautomerase. *Bioorg. Chem.* **2007**, *35*, 444−457.

(54) Hopmann, K. H.; Himo, F. Quantum Chemical Modeling of the Dehalogenation Reaction of Haloalcohol Dehalogenase. *J. Chem. Theory Comput.* **2008**, *4*, 1129−1137.

(55) Georgieva, P.; Himo, F. Quantum Chemical Modeling of Enzymatic Reactions: The Case of Histone Lysine Methyltransferase. *J. Comput. Chem.* **2010**, *31*, 1707−1714.

(56) Grimme, S.; Antony, J.; Ehrlich, S.; Krieg, H. A Consistent and Accurate Ab Initio Parametrization of Density Functional Dispersion Correction (DFT-D) for the 94 Elements H-Pu. *J. Chem. Phys.* **2010**, *132*, 154104−154119.

(57) Goodman, J. M.; Silva, M. A. QRC: A Rapid Method for Connecting Transition Structures to Reactants in the Computational Analysis of Organic Reactivity. *Tetrahedron Lett.* **2003**, *44*, 8233−8236.

(58) *LigPrep*, version 2.7; Schrödinger, LCC: New York, 2013.

(59) Shelley, J. C.; Cholleti, A.; Frye, L. L.; Greenwood, J. R.; Timlin, M. R.; Uchimaya, M. Epik: A Software Program for pKa Prediction and Protonation State Generation for Drug-like Molecules. *J. Comput.-Aided Mol. Des.* **2007**, *21*, 681−691.

(60) Friesner, R. A.; Banks, J. L.; Murphy, R. B.; Halgren, T. A.; Klicic, J. J.; Mainz, D. T.; Repasky, M. P.; Knoll, E. H.; Shelley, M.; Perry, J. K.; Shaw, D. E.; Francis, P.; Shenkin, P. S. Glide: A New Approach for Rapid, Accurate Docking and Scoring. 1. Method and Assessment of Docking Accuracy. *J. Med. Chem.* **2004**, *47*, 1739−1749.

(61) Halgren, T. A.; Murphy, R. B.; Friesner, R. A.; Beard, H. S.; Frye, L. L.; Pollard, W. T.; Banks, J. L. Glide: A New Approach for Rapid, Accurate Docking and Scoring. 2. Enrichment Factors in Database Screening. *J. Med. Chem.* **2004**, *47*, 1750−1759.

(62) *Glide*, version 6.3; Schrödinger, LCC: New York, 2014.

(63) *Phase*, version 3.6; Schrödinger, LCC: New York, 2013.

(64) Dixon, S. L.; Smondyrev, A. M.; Knoll, E. H.; Rao, S. N.; Shaw, D. E.; Freisner, R. A. PHASE: A New Engine for Pharmacophore Perception, 3D QSAR Model Development, and 3D Databases Screening: 1. Methodology and Preliminary Results. *J. Comput.-Aided Mol. Des.* **2006**, *20*, 647−671.

(65) *The PyMOL Molecular Graphics System*, version 1.6; Schrödinger, LCC: New York.

(66) Demaegdt, H.; Lenaerts, P.-J.; Swales, J.; De Backer, J.-P.; Laeremans, H.; Le, M. T.; Kersemans, K.; Vogel, L. K.; Michotte, Y.; Vanderheyden, P.; Vauquelin, G. Angiotensin AT4 Receptor Ligand Interaction with Cystinyl Aminopeptidase and Aminopeptidase N:

[125I]Angiotensin IV Only Binds to the Cystinyl Aminopeptidase Apo-Enzyme. *Eur. J. Pharmacol.* **2006**, *546*, 19−27.

(67) Demaegdt, H.; Vanderheyden, P.; De Backer, J.-P.; Mosselmans, S.; Laeremans, H.; Le, M. T.; Kersemans, V.; Michotte, Y.; Vauquelin, G. Endogenous Cystinyl Aminopeptidase in Chinese Hamster Ovary Cells: Characterization by [125I]Ang IV Binding and Catalytic Activity. *Biochem. Pharmacol.* **2004**, *68*, 885−892.